Colloid Polym Sci 276:1010–1018 (1998)

ORIGINAL CONTRIBUTION

Synthesis and characterization of surface-aminated polypyrrole–silica nanocomposites

M.I. Goller
C. Barthet
G.P. McCarthy
R. Corradi
B.P. Newby
S.A. Wilson
S.P. Armes
S.Y. Luk

Received: 19 May 1998
Accepted: 15 June 1998

M.I. Goller · C. Barthet · G.P. McCarthy
B.P. Newby · S.A. Wilson · S.P. Armes (✉)
School of Chemistry
Physics and Environmental Science
University of Sussex
Falmer Brighton BN1 9QJ
United Kingdom

S.Y. Luk
Analytical Division
Courtaulds Research
P.O. Box 111
101 Lockhurst Lane
Coventry, CV6 5RS
United Kingdom

Abstract Two synthetic routes to surface-aminated polypyrrole–silica nanocomposite particles have been investigated. Route 1 involved the initial synthesis of homopolypyrrole – silica particles as described previously, followed by surface amination using 3-aminopropyltriethoxy-silane. In Route 2 aminated polypyrrole–silica particles were synthesized directly by copolymerising an *N*-substituted aminopyrrole comonomer with pyrrole in the presence of an ultrafine silica sol. Both types of aminated particles were characterized in terms of their particle size and morphology, long-term colloid stability and degree of amination using transmission electron microscopy, disc centrifuge photosedimentometry and zeta potential measurements, respectively.

Key words Nanocomposite particle – homopolypyrrole silica – polypyrrole silica – copolymerising

Introduction

In a series of recent papers we have reported the preparation and characterisation of polyaniline–silica, polypyrrole–silica and polypyrrole–tin(IV) oxide particles using ultrafine silica or tin(IV) oxide sols as *particulate* dispersants in aqueous media [7–3]. These sols act as high surface area colloidal substrates for the precipitating polyaniline or polypyrrole, yielding stable colloidal dispersions of composite particles with a "raspberry" morphology. These colloidal "raspberries" consist of micro-aggregates of the silica (or tin(IV) oxide) sol held together by the conducting polymer binder component. Both the dimensions of the "raspberries" and the conducting polymer loading can be varied over a wide range by judicious selection of the oxidant type and silica concentration [4, 5, 7]. Small-angle X-ray scattering studies on polyaniline–silica raspberries have confirmed that these materials are true nanocomposites, since the polyaniline chains are confined within nanoscale cavities between the silica particles [8]. BET surface area measurements on a series of conducting polymer–inorganic oxides suggest that at least some of these nanocomposites exhibit significant micro-porosity [9].

XPS studies [10] of a series of conducting polymer–silica nanocomposites confirm that the conducting polymer component is always present at (or very near) the surface of the particles. On the other hand, their surface compositions were invariably silica-rich, as judged from their Si/N atomic ratios. Aqueous electrophoresis measurements [11] supported these observations since zeta potential vs. pH curves obtained for various polyaniline- and polypyrrole–silica nanocomposites are essentially superimposable on that of a silica sol. This is consistent with a charge stabilisation mechanism operating during both the initial formation of the nanocomposite particles and also their subsequent long-term colloid stability in aqueous media [12]. In this context it is noteworthy that silica sols, unlike many other oxide sols, are particularly resistant to electrolyte-induced flocculation [13]. This probably explains why so many other

oxide sols proved to be unsuitable dispersants for nanocomposite syntheses [6].

Polypyrrole–silica nanocomposites are promising new "marker" particles in immunodiagnostic strip assays [14]. In this context the "value-added" property is their intense intrinsic coloration, rather than their electrical conductivity. Other desirable characteristics are their small particle size, narrow size distribution and good colloid stability at physiological pH. One of the main problems in developing such assays is non-specific binding [15]. In principle, this can be overcome (or at least minimised) by incorporating hydrophilic functional groups such as carboxylic acids or amines onto the surface of the marker particles. This promotes specific covalent attachment of the analyte of interest. Recently, we have examined several synthetic routes for the surface functionalisation of our polypyrrole-silica nanocomposites. Carboxylated nanocomposites have been successfully prepared simply by copolymerising a functional pyrrolic comonomer (either 1-(2-carboxyethyl)pyrrole or pyrrole-3-acetic acid) with pyrrole during the nanocomposite synthesis[16, 17]. Subsequent X-ray photoelectron spectroscopy studies confirmed that the carboxylic acid groups are located at the surface of the particles, as expected. In a collaborative study with Tarcha's group at Abbott Laboratories [18], it was demonstrated that carboxylic acid–functionalized polypyrrole–silica particles could be used as marker particles in a simple strip assay for the human pregnancy hormone, hCG.

In the present work we describe our attempts to synthesize surface-aminated polypyrrole–silica particles. Two synthetic routes were examined. Route 1 (see Fig. 1) involved functionalization of homopolypyrrole–silica nanocomposite particles using 3-aminopropyltriethoxysilane reagent (APTES). Route 2 (see Fig. 2) involved

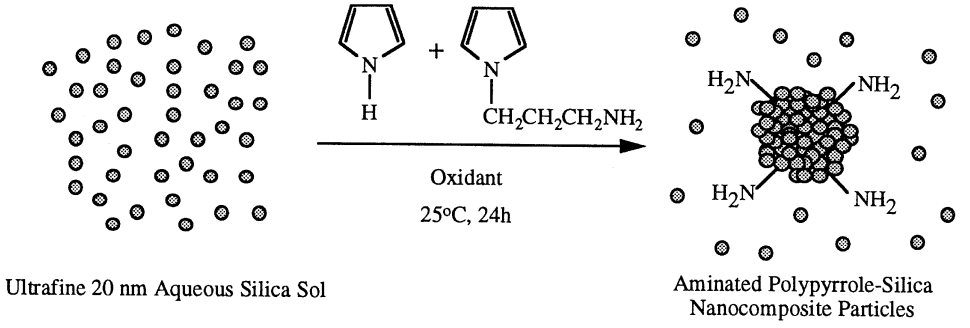

Fig. 1 Schematic representation of the synthesis of aminated polypyrrole–silica nanocomposite particles via Route 1

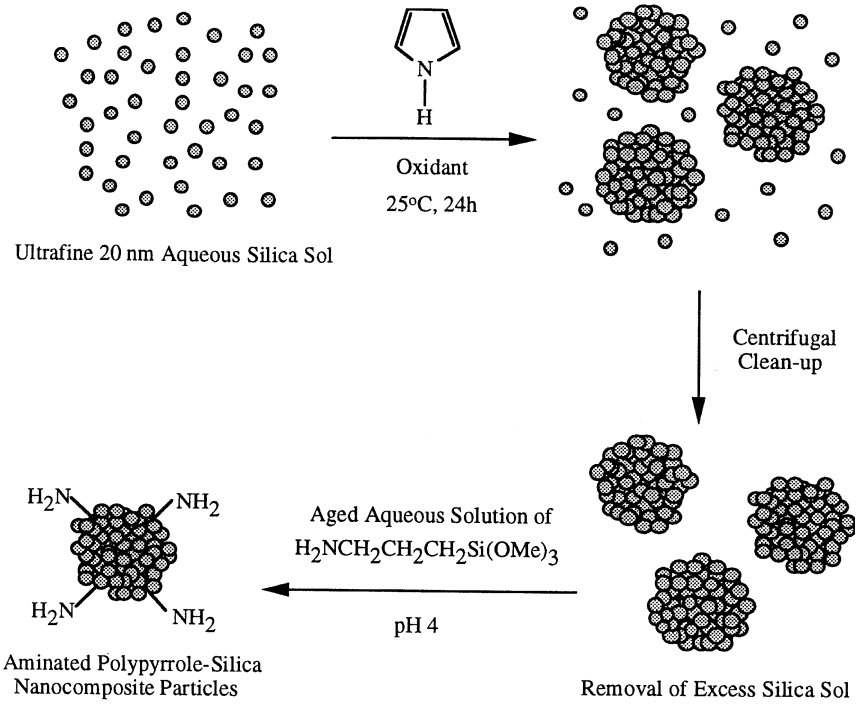

Fig. 2 Schematic representation of the synthesis of aminated polypyrrole–silica nanocomposite particles via Route 2

copolymerization of an amine-functionalized pyrrolic comonomer with pyrrole in the presence of an ultrafine silica sol. The resulting dispersions have been extensively characterized in terms of their particle morphology and size distribution, silica content, colloid stability and surface composition using transmission electron microscopy, disc centrifuge photosedimentometry, thermogravimetric analysis, zeta potential measurements, surface-enhanced Raman spectroscopy and X-ray photoelectron spectroscopy, respectively.

Experimental

Materials

Pyrrole, 1-(2-cyanoethyl)pyrrole, ammonium persulfate, iron(III) chloride, lithium aluminium hydride (1.0 M solution in diethyl ether), anhydrous diethyl ether, sodium chloride, potassium hydroxide and acetic acid were obtained from Aldrich. Pyrrole was passed through a column of basic alumina and stored at 4 °C prior to use. Aqueous silica sol (*Nyacol* 2034DI), with a nominal particle size of 20 nm, was kindly donated by Eka Chemicals (Sweden). 3-aminopropyltriethoxysilane (APTES) was obtained from OSi Specialities Ltd. Water was de-ionized and doubly distilled.

Synthesis of nanocomposites

The preparation of homopolypyrrole–silica nanocomposites involved the addition of pyrrole to an aqueous silica sol in the presence of a chemical oxidant [4, 5, 7]. Thus, pyrrole (1.0 ml) was added to a vigorously stirred dispersion of colloidal silica (3.47 w/v%) in deionized water containing $(NH_4)_2S_2O_8$ (3.84 w/v%) as oxidant. Subsequently, the mixture was stirred for a further 24 h to allow the pyrrole polymerization to proceed to completion. The resulting colloidal nanocomposite particles were isolated from the soluble inorganic byproducts and excess silica sol via four centrifugation/redispersion cycles (6000 rpm for 30 min), with successive supernatants being replaced with water.

Nanocomposite preparation via copolymerisation

The 1-(3-aminopropyl)pyrrole comonomer was synthesised by the reduction of 1-(2-cyanoethyl)pyrrole in anhydrous diethyl ether [19]. 1-(2-cyanoethyl)pyrrole (5–10 g) was added dropwise to a two molar excess of $LiAlH_4$ (1.0 M solution in anhydrous diethyl ether) (total solvent volume 344 ml). The reaction was stirred under nitrogen for 2 h and then quenched by successive additions of water, sodium hydroxide (20 wt%) and water. The ethereal layer was decanted and the product was collected as a yellow oil after evaporation of the ether phase. The comonomer was characterised by ^1H NMR spectroscopy using a 250 MHz instrument ($CDCl_3$ solvent and TMS reference).

The preparation of poly(pyrrole-*co*-1-(3-aminopropyl)pyrrole–silica nanocomposites involved incorporation of the comonomer into the experimental protocol described above. Thus, pyrrole and 1-(3-aminopropyl)pyrrole were pre-mixed in 75 : 25 and 50 : 50 volume ratios. This comonomer mixture (0.32 g) was then added to a vigorously stirred solution containing the silica sol (ca. 4 g dry weight silica) and $FeCl_3$ (3.04 g) in 40 ml de-ionized water. The solution was stirred at 25 °C for 24 h. The resulting colloidal nanocomposites were isolated by four centrifugation/redispersion cycles and redispersed in de-ionized water.

Silylation of nanocomposites

Surface silylation of the pre-formed polypyrrole–silica particles was accomplished using a procedure described by Goodwin et al. [20]. Nanocomposite particles (3.1 wt%) were functionalized by the addition of APTES (1 wt%) at pH 4 (adjusted by the addition of acetic acid) for 2 h at 25 °C. The resulting silylated sols were purified by four centrifugation/redispersion cycles at 4000 rpm for 40 min and were redispersed in 0.01 M aqueous NaCl solution, adjusted to pH 4 with 0.1 M HCl.

Nanocomposite composition

The silica contents of the nanocomposites were determined by thermogravimetric analysis (TGA) using a Perkin-Elmer TGA-7 instrument at a scan rate of 20 °C min^{-1} in air. After complete pyrolysis of the conducting polymer, the remaining residues were assumed to be solely due to the incombustible silica component. A small correction was made to allow for the moisture content of the silica sol (ca. 10%).

Nanocomposite morphology

Nanocomposite particle morphology and average particle diameters were assessed using a Hitachi 7100 transmission electron microscope. A dilute dispersion of the nanocomposite particles was dried onto a carbon-coated copper grid.

Particle size determination

Weight-average particle diameters and size distributions were determined by disc centrifuge photosedimentometery (DCP) using a Brookhaven instrument operating in the external line-start mode [2]. The densities of the dried nanocomposites, required for DCP analysis, were measured using a Micrometrics *AccuPyc* 1330 helium pycnometer. DCP was also used to assess the degree of dispersion of the nanocomposites on long-term storage at 25 °C in solutions of varying pH.

Microelectrophoretic measurements

Electrokinetic data were obtained using a Malvern *ZetamasterS* instrument. Zeta potentials were calculated from mobilities using the Henry equation and determined as a function of solution pH (background ionic strength 0.01 M NaCl; 25 °C). The pH was adjusted by the addition of HCl and NaOH. The silica particles (kindly donated by Merck, UK; Monospher 250) which were used as a reference material for the amination experiments had a particle diameter of approximately 250 nm.

Surface-enhanced Raman spectroscopy (SERS)

One drop of a dilute suspension of the polypyrrole–silica nanocomposite particles was spin-coated at sub-monolayer concentration onto an aluminium stub which had been roughened with 400 mesh carborundum paper. This was then sputter-coated with a thin (ca. 70 nm) overlayer of silver at 10^{-5} torr prior to recording a SERS spectrum. This experiment was repeated for a dilute dispersion of aminated polypyrrole–silica particles prepared using APTES according to Route 1. Control experiments undertaken in the absence of the gold overlayer gave no Raman signals, indicating that the results obtained were due to a genuine SERS effect and not normal Raman scattering. A Bruker FRA 106 spectrometer equipped with a 1064 nm laser was used to record the SERS spectra (typically averaged over 2000 scans at 8 cm^{-1} resolution).

X-ray photoelectron spectroscopy (XPS)

Spectra were obtained from compressed pellets of homopolypyrrole–silica particles and aminated polypyrrole–silica particles (obtained via Route 1) using a Kratos Prism X-ray photoelectron spectrometer (unmonochromated 1254 eV Mg Kα source and a vacuum of at least 10^{-8} torr). Samples were mounted on a stainless-steel bar using double-sided adhesive tape. Survey scans were recorded at a pass energy of 80 eV, with a 0.1 eV step and a dwell time of 300 ms. All peaks were referenced against the *C*1s peak at 284.7 eV.

Results and discussion

The main advantage of Route 1 is that the precursor homopolypyrrole–silica particles can be readily prepared with relatively narrow size distributions [5, 7]. Since such particles are known to have silica-rich surfaces [10], the protocol described by Goodwin et al. [20] for the amination of silica sols should be readily applicable. The potential advantage of Route 2 is that the aminated particles are synthesised in a single step. However, the amine-functionalized pyrrole comonomer required for Route 2 is not commercially available and therefore had to be synthesised. A summary of the synthesis conditions and the properties of the aminated polypyrrole–silica particles is provided in Table 1.

Transmission electron micrographs of the aminated polypyrrole–silica particles obtained from Routes 1 and 2 are shown in Fig. 3. The particle morphologies are clearly different. Route 1 produces "raspberry" particles which are

Table 1 Effect of synthesis conditions on the particle size distributions, isoelectric points and silica contents of the aminated polypyrrole–silica nanocomposite particles prepared via Routes 1 and 2

	Pyrrole:aminopyrrole comonomer ratio	Silica w/v%	Oxidant type	Weight-average DCP diameter/nm	i.e.p.	Silica content/wt%[b)]
PPy–SiO_2	100:0	1.73*	$(NH_4)_2S_2O_8$	113 ± 12	≈ 2.0	54.9
PPy–SiO_2–APTES	100:0	1.73	$(NH_4)_2S_2O_8$	159 ± 30[a)]	7.5	—
COP–SiO_2	75:25	9.5	$FeCl_3$	348 ± 150	8.5	25.8
COP–SiO_2	50:50	11.5	$FeCl_3$	215 ± 60	9.0	10.7

[a)] The increase in particle diameter after amination indicates some degree of flocculation.
[b)] As determined from thermogravimetric analysis in air at 20 °C per minute.

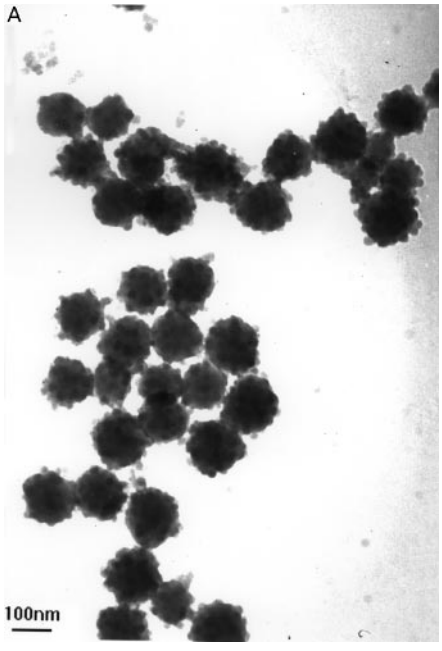

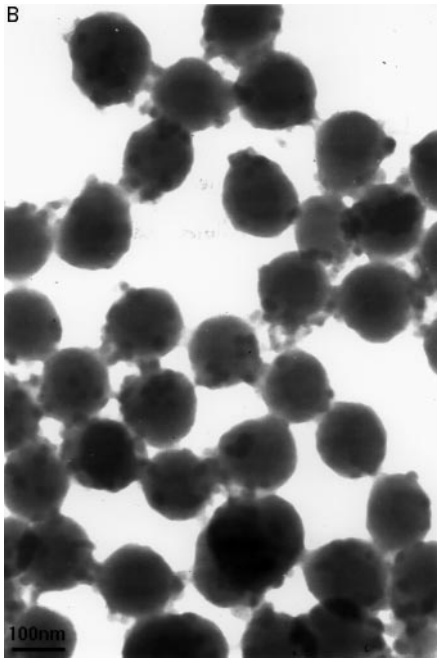

Fig. 3 Representative transmission electron micrographs for aminated polypyrrole–silica nanocomposite particles obtained from (A) Route 1 and (B) Route 2. Note the difference in particle morphology: "raspberry" particles are obtained from Route 1 (APTES treatment) whereas more spherical particles are obtained from Route 2 (copolymerisation)

indistinguishable from the homopolypyrrole –silica precursor particles prior to surface amination using APTES. On the other hand, the particles obtained via Route 2 are much more spherical. This latter observation is consistent with

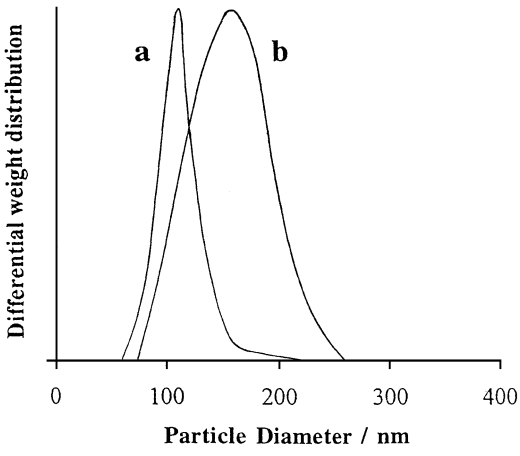

Fig. 4 Weight-average particle size distributions obtained using the disc centrifuge photosedimentometer for homopolypyrrole–silica nanocomposite particles (a) before APTES and (b) after APTES treatment. The apparent increase in particle diameter indicates incipient flocculation of the aminated particles, rather than an actual increase in particle size

that reported by both Maeda et al. [16] and McCarthy et al. [17], who each obtained relatively spherical morphologies for composite particles prepared by copolymerising carboxylic acid–functionalized pyrrole comonomers with pyrrole in the presence of ultrafine silica sols. The smoother, more spherical morphologies are also consistent with the relatively low silica contents (10.7 and 25.8%, respectively) of the aminated particles obtained via Route 2. In contrast, the surface-rough raspberry particles obtained from Route 1 have a much higher silica content. The primary particle size for both types of aminated polypyrrole–silica particles is in the 100–150 nm range as judged by transmission electron microscopy. However, DCP analyses indicate differing degrees of dispersion (see Table 1). The homopolypyrrole–silica particles become weakly flocculated on amination with APTES (see Fig. 4), with the weight-average particle diameter increasing from 113 ± 12 nm to 159 ± 30 nm. It is noteworthy that Giesche and Matijevic also reported [21] incipient flocculation of similar-sized silica sols treated with APTES, although in their case this aggregation appeared to be reversible. Comparison of the DCP data obtained for the aminated particles synthesized via Route 2 with their TEM particle diameters indicates that both these dispersions (see entries 3 and 4 in Table 1) are weakly flocculated.

Zeta potential vs. pH curves for aminated polypyrrole–silica particles, aminated silica particles and a reference silica sol are presented in Fig. 5. The silica sol has an isoelectric point at around pH 2 in accordance with the literature [11], whereas the APTES-treated silica has an isoelectric point at around pH 6.5. The aminated

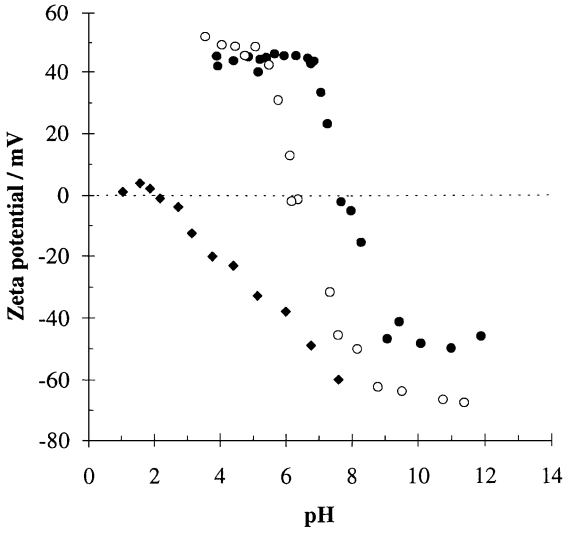

Fig. 5 Zeta potential vs. pH data for: (♦) a silica sol (Monospher 250, ex. E. Merck); (○) the aminated silica sol obtained after APTES treatment; (●) aminated polypyrrole–silica nanocomposite particles obtained after APTES treatment

polypyrrole–silica particles also exhibit a classical 'S' shaped curve. This confirms successful surface amination of the particles, since the positive zeta potentials found in acidic media are due to protonation of the surface amine groups. The observed isoelectric point at pH 7.5 is comparable to the isoelectric points reported by Goodwin et al. [20] using the same APTES derivatization protocol, but lower than the isoelectric point of pH 9–9.5 obtained by Giesche and Matijevic, who preferred a mixed APTES/ammonia/ethanol/water solution for surface functionalization [21]. X-ray photoelctron spectroscopy studies were also consistent with surface amination (see below).

X-ray photoelectron spectroscopy (XPS)

The X-ray photoelectron survey spectra for the homopolypyrrole–silica nanocomposite prior to and after amination with APTES are shown together in Fig. 6. The N1s signal at ca. 400 eV clearly becomes more intense relative to the other peaks after amination. In order to quantify this effect we determined N/Si atomic ratios from the respective N1s and Si2p coreline spectra (not shown). The N/Si atomic ratio increased from 0.05 for the homopolypyrrole–silica particles to 0.22 for the APTES-treated particles. Given that XPS is a highly surface-specific technique with a typical analysis depth of 5–10 nm, these observations confirm the presence of surface amine groups on the polypyrrole–silica particles after APTES treatment.

Route 2 also produced aminated polypyrrole–silica particles. Zeta potential data (not shown) obtained for nanocomposites synthesised using a comonomer feed of 50 mol% 1-(3-aminopropyl)pyrrole (entry 4 in Table 1) indicated an isoelectric point at pH 9, whereas the particles synthesized using 25 mol% 1-(3-aminopropyl)pyrrole (entry 3 in Table 1) had a isoelectric point at 8.5. Thus a higher surface concentration of amine groups was obtained using a higher proportion of 1-(3-aminopropyl)pyrrole in the comonomer feed, as expected. In this context, it is

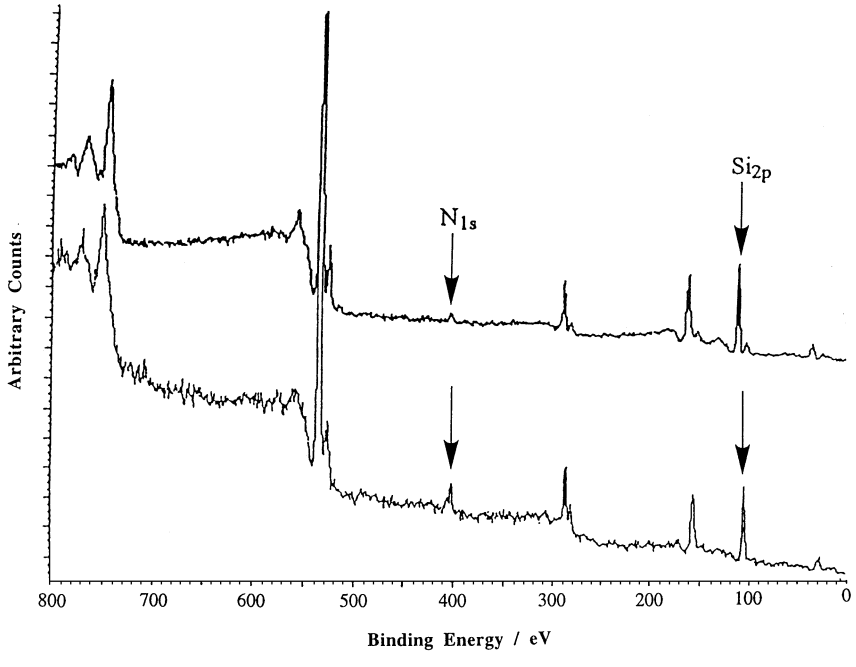

Fig. 6 Survey X-ray photoelectron spectra for homopolypyrrole–silica nanocomposite particles before APTES treatment (upper spectrum) and after APTES treatment (lower spectrum). Note the increased intensity of the N1s signal relative to the Si2p signal, which confirms successful surface amination

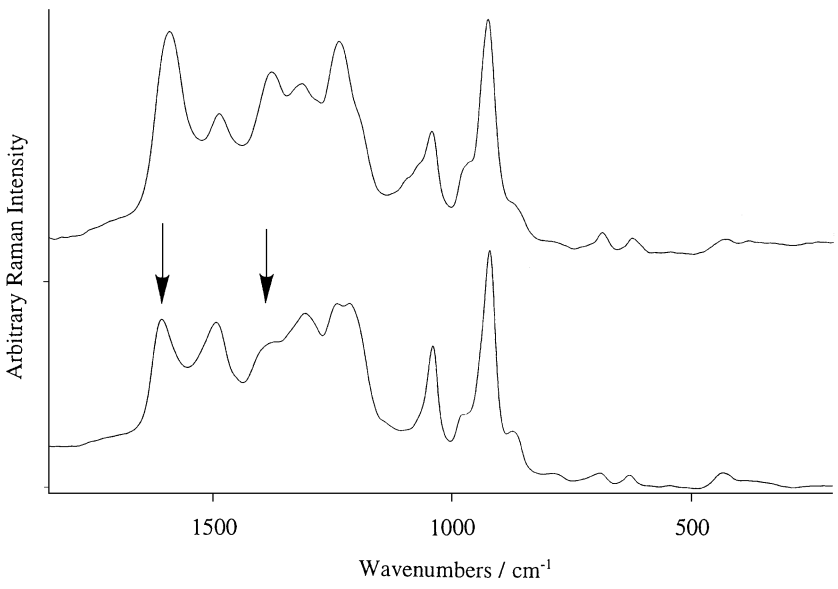

Fig. 7 Surface-enhanced Raman spectra obtained from homopolypyrrole–silica particles (upper spectrum) and APTES-treated polypyrrole–silica particles (lower spectrum). Note the reduced intensities of the two bands at 1588 and 1388 cm^{-1} which is consistent with surface de-doping of the polypyrrole chains by the APTES

noteworthy that highly aminated polypyrrole–silica particles cannot be obtained by simply replacing all of the pyrrole with the 1-(3-aminopropyl)pyrrole comonomer since homopoly(1-(3-aminopropyl)pyrrole) is too water-soluble under the synthesis conditions to act as a binder for the silica sol [22].

Surface-enhanced Raman scattering (SERS)

SERS spectra obtained from unfunctionalised and aminated polypyrrole–silica particles deposited at submonolayer coverage on a silver-coated, roughened surface are shown together in Fig. 7. Since SERS is highly surface-specific [23], these Raman spectra should should be representative of only the surfaces of the nanocomposite particles which are in intimate contact with the silver overlayer. The strong polypyrrole signature in the Raman spectrum of the unfunctionalized polypyrrole–silica particles is identical to that reported in the literature [24, 25] and confirms that the conducting polymer component must be located at (or very near) the surface of the particles. This is in good agreement with an earlier XPS study on a series of polypyrrole–silica nanocomposites reported by Maeda et al., who observed N1s signals due to the polypyrrole components in each case [10]. It is noteworthy that there are no Raman features which can be assigned to silica since this component produces only very weak Raman scattering. The SERS spectrum of the aminated polypyrrole–silica particles obtained using APTES (Route 1) is markedly different to that of the unfunctionalised homopolypyrrole–silica particles. In particular, the relative intensities of the two bands at 1588 and 1380 cm^{-1} are markedly reduced compared to that of the 1488 cm^{-1} band. These spectral changes are consistent with a significant degree of de-doping of the cationic polypyrrole chains at the surface of the nanocomposite particles [26]. With the benefit of hindsight, this observation is not particularly surprising since it is well known that even weak bases such as aliphatic amines (e.g. APTES) are sufficient to de-dope polypyrrole [27]. It is worth emphasising that, with the possible exception of XPS (which would involve very careful peak deconvolution), SERS is probably the only analytical technique capable of confirming surface-dedoping of the polypyrrole chains by the APTES.

Long-term colloid stability of the dispersions

The degree of flocculation of the aminated particles obtained by Routes 1 and 2 increased irreversibly on long-term storage at room temperature, eventually leading to precipitation of the particles after several weeks. Attempts to improve colloid stabilities by varying the solution pH (pH 4, 7 and 10 were investigated) proved fruitless. There was a good correlation between loss in colloid stability and reduction in zeta potential. For example, a fresh dispersion of aminated particles obtained via Route 1 had an initial zeta potential of +45 mV (see Fig. 8A). The zeta potential of this dispersion decreased monotonically to less than +25 mV after three weeks storage at pH 4 and room temperature. An even more marked reduction (from +30 to +8 mV) was observed within one week at pH 10. Similar observations were reported by Goodwin et al., who attributed the reduction in zeta potential to hydrolysis of the surface APTES groups [20]. However, similar, albeit

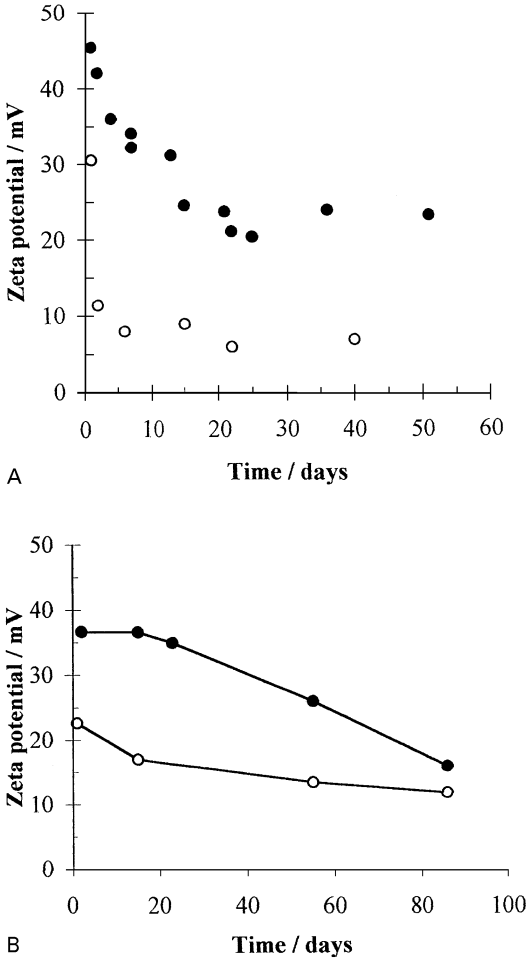

Fig. 8 (A) Variation of zeta potential of APTES-treated polypyrrole–silica particles obtained from Route 1 on long-term storage at (●) pH 4 and (○) pH 10; (B) Variation of zeta potential of aminated polypyrrole–silica particles obtained from Route 2 on long-term storage at (●) pH 4 and (○) pH 10

slower, systematic reductions in zeta potential were also observed for the colloidally unstable aminated particles obtained via Route 2 (see Fig. 8B). In this case the amine groups are covalently attached via carbon–carbon bonds to the copolymer component of the nanocomposite and it is therefore more difficult to envisage a plausible hydrolysis mechanism.

Conclusions

Zeta potential measurements confirm the successful synthesis of surface-aminated polypyrrole–silica nanocomposite particles by both Routes 1 and 2. Isoelectric points at pH 8.5 to 9.0 were obtained via Route 2, which suggests that this method produces the highest degree of surface amination. X-ray photoelectron spectroscopy studies confirm the presence of amine groups at the surface of APTES-treated polypyrrole–silica particles. In addition, SERS studies reveal some degree of surface de-doping of the conducting polymer component occurs via Route 1. Disc centrifuge photosedimentometry data indicate that incipient flocculation of the polypyrrole–silica particles occurs during surface amination using APTES.

TEM studies indicate that the aminated polypyrrole–silica particles obtained via Route 2 have a more spherical morphology than the "raspberry" particles produced by Route 1. Unfortunately, neither Route 1 nor 2 produced aminated polypyrrole–silica particles with acceptable long-term colloid stability. The observed reduction in zeta potential over a time-scale of weeks correlated quite well with the observed irreversible aggregation of these dispersions. With the APTES-modified particles obtained from Route 1 this reduction in zeta potential presumably corresponds to the slow hydrolysis of the APTES groups. Varying the solution pH during storage did not prevent particle aggregation. Unless their shelf-life can be improved significantly, these particles are unlikely to be useful as marker particles in immunodiagnostic assays.

Acknowledgements This work was supported by EPSRC (GR/K01841) which provided post-doctoral grants for MIG and GMcC. CB thanks the EC Training and Mobility of Researchers programme for a Marie-Curie fellowship.

References

1. Gill M, Mykytiuk J, Armes SP, Edwards JL, Yeates T, Moreland PJ, Mollett C (1992) J Chem Soc Chem Commun 108–109
2. Gill M, Armes SP, Fairhurst D, Emmett SN, Idzorek GC, Pigott T (1992) Langmuir 8:2178–2182
3. Stejskal J, Kratochvil P, Armes SP, Lascelles SF, Riede A, Helmstadt M, Prokes J, Krivka I (1996) Macromolecules 29: 6814–6819
4. Maeda S, Armes SP (1993) J Colloid Interface Sci 159:257–259
5. Maeda S, Armes SP (1994) J Mater Chem 4:935–942
6. Maeda S, Armes SP (1995) Chem Mater 7:171–178
7. Lascelles SF, Butterworth MD, McCarthy GP, Armes SP (1998) Colloid Polymer Sci, in the press
8. Terrill NJ, Crowley T, Gill M, Armes SP (1993) Langmuir 9:2093–2096
9. Maeda S, Armes SP (1995) Synth Met 73:151–155
10. Maeda S, Gill M, Armes SP, Fletcher IW (1995) Langmuir 11:1899–1904
11. Butterworth MD, Corradi R, Johal J, Maeda S, Lascelles SF, Armes SP (1995) J Colloid Interface Sci 174: 510–517
12. Hunter RJ (1987) In: Foundations of Colloid Science, Vol I. Clarendon Press, Oxford

13. Healy TW (1990) In: Berga HE (ed) The Colloid Chemistry of Silica. ACS Symp Ser No. 234, American Chemical Society, Washington DC, USA
14. Armes SP, Maeda S (1994) ACS Polym Prepr 35 (1):217–218
15. Tarcha PJ, Misun D, Finley D, Wong M, Donovan JJ (1992) In: Daniels ES, Sudol ED, El-Aassar MS (eds) Polymer Latexes: Preparation, Characterisation and Applications, Vol 22. ACS Symp Ser (492) pp 347–367
16. Maeda S, Corradi R, Armes SP (1995) Macromolecules 28:2905–2911
17. McCarthy GP, Armes SP, Greaves SJ, Watts JF (1997) Langmuir 13:3686–3692
18. Pope MR, Armes SP, Tarcha PJ (1996) Bioconjugate Chem 7:436–444
19. Foulds NC, Lowe CR (1988) Anal Chem 60:2473–2478
20. Goodwin JW, Harbron RS, Reynolds PA (1990) Colloid Polym Sci 268:766–777
21. Giesche H, Matijevic E (1991) Dyes and Pigments 17:323–340
22. Maeda S, Corradi R, Armes SP, unpublished results
23. Cotton TM, Kim J-H, Chumanov GD (1991) J Raman Spectroscopy 22:729–742
24. Luk SY, Keane M, Lineton W, DeArmitt C, Armes SP (1995) J Chem Soc Faraday Trans 91(5):905–910
25. Bjorklund RB, Maeda S, Armes SP, Luk SY (1998) J Colloid Interface Sci 197: 179–184
26. Jenden CM, Davidson RG, Turner TG (1993) Polymer 34:1649–1652
27. Foot P, Ritchie T, Mohammad F (1988) J Chem Soc Chem Commun 1536–1537